Sensors & Transducers, Vol. 256, Issue 2, March 2022, pp. 12-18

www.sensorsportal.com

Sensors & Transducers

Published by IFSA Publishing, S. L., 2022
http://www.sensorsportal.com

Symmetry-based Method for Water Level Prediction using Sentinel 2 Data

[1, *] David JESENKO, [2] Lukáš HRUDA, [2] Ivana KOLINGEROVÁ, [1] Borut ŽALIK and [1] David PODGORELEC

[1] University of Maribor, Faculty of Electrical Engineering and Computer Science, Koroška cesta 46, SI-2000 Maribor, Slovenia
[2] University of West Bohemia, Faculty of Applied Sciences, Department of Computer Science and Engineering, Technická 8, 301 00, Plzeň, Czech Republic
[*] Tel.: +386-2-220-7476, fax: +386-2-220-7272
[*] E-mail: david.jesenko@um.si

Received: 31 January 2022 /Accepted: 1 March 2022 /Published: 31 March 2022

Abstract: The Sentinel satellite constellation series, developed and operated by the European Space Agency, represents a dedicated space component of the European Copernicus Programme, committed to long-term operational services in the environment, climate and security. A huge amount of acquired data allow us different surveys. The paper considers the detection of changes in water levels in Lake Cerknica. The multispectral index has been calculated from Sentinel-2 data and transformed to a 3D point cloud. As shown by the results, symmetry measures of 3D point clouds could be used for the detection of water levels. Prediction functions using a genetic algorithm have been fitted, and the best result achieved was RMSE = 0.9824.

Keywords: Sentinel-2, Lake Cerknica, Remote sensing, Water monitoring, Symmetry, Symmetry measure, Genetic algorithm.

1. Introduction

Monitoring open water bodies accurately is an important task and one of the basic applications in Remote sensing. They are a significant part of the Earth's water cycle, and water bodies such as rivers, lakes and reservoirs are irreplaceable for the global climate system and the ecosystem. Remote sensing has become a conventional approach for monitoring water bodies, as it is often real-time, dynamic and cost-effective [1]. The measuring and monitoring of surface water using Remote sensing technology is, therefore, an essential topic [2]. In particular, the use of freely available high-spatial resolution optical satellite data is relevant [3]. Such data include the images obtained by the Landsat series [4-6], Advanced Spaceborne Thermal Emission and Reflection Radiometer (ASTER) [7-8], and Sentinel-2 [1, 9] multispectral imagery. A high extraction accuracy has been achieved in the mapping of surface water bodies, including lakes [10], rivers [11], coastlines [12] and water bodies in rural areas [13].

Among all the existing water body mapping methods, the calculation of a multispectral index is the most reliable, as it is user-friendly, efficient and has low computational cost [14]. The use of the water index is currently accepted to enhance the differences between water and non-water bodies, based on combinations of two or more spectral bands using various algebraic operations [15]. The well-known Normalised Difference Water Index (NDWI) [13] is sensitive to built-up lands, and frequently results in the

overestimation of water bodies in urban areas [16]. The modified NDWI (MNDWI) [17] is used mostly in urban scenes to improve the separability of the built-up areas. The Automated Water Extraction Index (AWEI) [18] highlights the water bodies in urban areas against shadowed and dark surfaces. It consists of two separate indices, one for areas where shadow is not important, and a second one, where shadow is significant.

A number of methods exist that are designed to seek symmetries in 3D objects. Some aim to detect symmetries of rather general types, including reflectional ones such as [19] or the well-known [20] and its newer modification [21]. However, when trying to find specifically reflectional symmetries it is usually more convenient to employ methods that specialise in detecting this type of symmetry. Since reflectional symmetry is probably the most occurring symmetry type in real world objects, there are quite a few such methods, such as [22-25] among the older ones. The more recent ones include [26-31]. For our purpose we chose among the newer methods and selected the method of Hruda et al. [31] because it is recent, appears to be robust, fast and only requires a set of points on the input which is not the case with some other methods. A detailed description of the method [31] follows in the next Section.

The observed water unit in the presented paper is Lake Cerknica. It is one of the largest intermittent lakes in Europe. Lake Cerknica is located in the southwestern part of Slovenia, caught between the Javorniki hills and the Bloke plateau on one side, and Mount Slivnica on the other. It appears every year on the karst plain, and is present for about eight months of the year. Water usually spreads over a surface of 20 km2, but, at its fullest, the lake covers a surface of about 26 km2. The height above sea level is in the range from 546 m to 551 m, with the maximum depth about 10 m. When full it is the largest lake in Slovenia [32]. The lake is an important wildlife resort, especially as a nesting place for many bird species. During the dry season the lake disappears, which enables hiking and grass mowing, but, on the other hand, while present, allows for paddling and fishing. For these reasons it is crucial to detect water levels at different times of the year.

The methodology used in the presented paper is described in Section 2. The results are given in Section 3, while Section 4 concludes the paper.

2. Methodology

This Section presents the methodology used in this paper to determine the water levels in Lake Cerknica using Sentinel-2 data and symmetry measure [33]. Firstly, the Sentinel-2 data were acquired from the European Space Agency's (ESA) official website, then the multispectral index was calculated, followed by extraction of the area of Lake Cerknica from the multispectral index and calculation of the symmetry measure of the lake. The water level of Lake Cerknica is predicted finally. Each of these steps is explained additionally in the continuation. A flowchart of the proposed method is represented in Fig. 1.

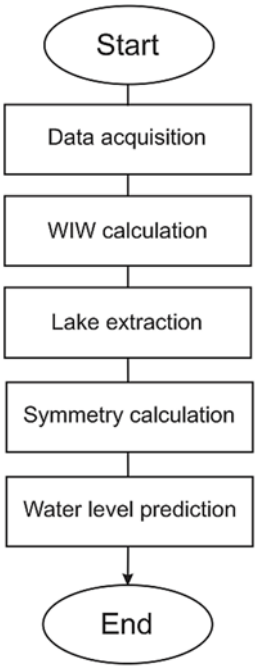

Fig. 1. Flowchart of the proposed approach.

Sentinel-2 data are composed of 13 spectral bands, that range from the visible range to the shortwave infrared. Data are freely available on the ESA website, accessible at https://scihub.copernicus.eu. The multispectral index, named the Water In Wetlands index (WIW), was calculated from the acquired data [33]. The WIW (Eq. 1) is defined by:

$$WIW = B8A \leq 0.1804 \;\&\&\; B12 \leq 0.1131, \quad (1)$$

where B8A represents a narrow Near Infra-Red (NIR) band, and B12 is a Short Wave Infra-Red (SWIR) band. In other words, flooded areas could be distinguished from dry areas when the pixels satisfy the conditions in Eq. 1 [34].

The area of Lake Cerknica was extracted using a mask, which, in the detail, describes the entire area of the lake. The extracted pixels from the WIW index were converted from 2D to 3D in such a way that a pixels with x and y coordinates, contained in the area of the flooded lake, store the intensity (coordinate z) of the WIW index.

2.1. Symmetry Estimation

The symmetry was calculated using the method presented in [31]. The method is designed to find the plane of reflectional symmetry of a 3D point set, and is based on maximizing an objective function called symmetry measure. Having a set of points

$X = \{x_1, x_2, \ldots, x_n\}$, $x_i \in E^3$, $i = 1, \ldots, n$, and a plane $P: ax + by + cz + d = 0$ represented by a vector $p = [a, b, c, d]^T$ the symmetry measure is defined as follows (Eq. 2):

$$s_X(p) = \sum_{i=1}^{n} \sum_{j=1}^{n} \varphi\left(\left\| r(p, x_i) - x_j \right\|\right), \quad (2)$$

where $r(p, x) \in E^3$ is a function that reflects a point $x \in E^3$ over the plane represented by p, and $\varphi(l)$ is a locally supported differentiable Wendland's function [35] which resembles the Gaussian for $l \geq 0$, and basically measures the similarity of two points based on their distance. Each point of the point set X is reflected over the plane represented by p and its similarity is computed to all points. All these similarities are summed together, providing the symmetry measure value. The idea behind the method is that maximizing the symmetry measure for p should maximise the similarity of the point set to its reflected version, and therefore maximize the symmetry over the plane represented by p. Since φ is locally supported, the distances only need to be computed for nearby points, and the computation of the symmetry measure can easily be accelerated using a 3D grid. Also, the symmetry measure is differentiable with regard to p, so any gradient-based optimization technique can be employed to locate its maximum.

Having the input point set X, two simplified versions are created, one denoted X_{simp} with approximately 1,000 points intended for the symmetry measure computation, and one denoted X_{cand} with roughly 100 points for candidate creation. The number of symmetry plane candidates are created by pairing points of X_{cand}, and each candidate p_i is evaluated by the symmetry measure $s_{X_{simp}}(p_i)$. Subsequently, S candidates with the largest value of the symmetry measure are selected, and local numerical optimization using the L-BFGS method [36] is started from all of them. This provides S local maxima of the symmetry measure $s_{X_{simp}}$, and selecting the one with the largest measure value results in the final symmetry plane.

2.2. Genetic Algorithm

This subsection presents an evolutionary algorithm, more precisely a genetic algorithm, for finding the most suitable predictive function [37, 38]. The function will predict the water level in Lake Cerknica based on estimated symmetry measure in the previous subsection. The task of the genetic algorithm is estimation of the coefficients for the predictive function. In a genetic algorithm the coefficients are represented as individuals. The process of estimation of coefficients consists of a few main steps, which are, generation of the initial population, selection, crossover, mutation, evaluation of individuals and the stopping criteria. A flowchart and the main steps can be seen in Fig. 2. In the continuation each of the main steps will be explained in detail.

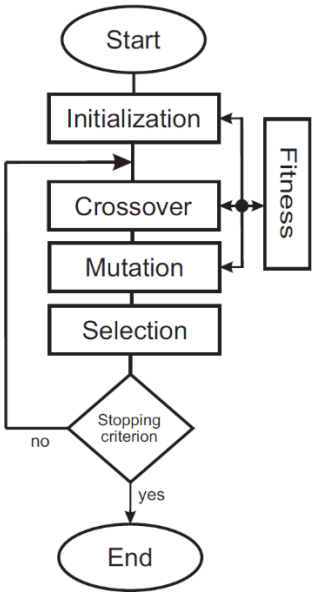

Fig. 2. Flowchart of the proposed genetic algorithm.

As mentioned, the following steps are in charge of finding the most suitable solution:

- **The initial population** was generated first. It consists of a set of randomly generated individuals. Each individual consists of chromosomes, and each chromosome represents a completely randomly generated coefficient for the predictive function.
- **Selection** of the individuals is a very important step towards finding the most suitable solution (predictive function). The tournament selection of size two is used, which means, that two individuals from the population are selected and compared, and, finally, the one with the best fitness, in our case the lowest Root-Mean-Square Error (RMSE), continues into the next generation.
- **Crossover** is used to generate new individuals and develop the population by combining the fittest individuals (chromosomes) from the previous generation. Two parents were selected randomly from the population, and a new individual was generated by copying the chromosomes from the first or the second parent. A two-point crossover was applied, which means that two crossover points are picked randomly from the parents and the chromosomes were swapped between the two points.
- **Mutation** is performed over randomly chosen individuals from the population, to allow new genetic material to enter, and, thus, keep the population diverse. Chromosomes from individuals are also selected randomly, and modified by a small positive or negative value.
- **Evaluation of individuals,** also called a fitness function, is performed by measuring the efficiency of the forecast made by each individual, which serves as the predictive function. Efficiency is measured by the already mentioned RMSE.

- **Stopping criteria** terminates the execution of the genetic algorithm. Three different criteria have been used. The first one, which is almost never achieved in practice, is when RMSE is equal to 0, the second one occurs when the minimal RMSE is not changed in five consecutive generations. The last one is triggered when 4,000 individuals are evaluated. If the stopping criteria are not satisfied, the proposed genetic algorithm repeats the basic steps (crossover, mutation, and selection).

3. Results

3.1. Parameter Sensitivity

The proposed method (genetic algorithm) for prediction relies on five input parameters. These parameters are the size of the population, the probability of crossover, the probability of mutation, the coefficients' change range, and the number of individual evaluations. In order to examine their influences on the method performance and estimate their optimal values, a systematic sensitivity analysis was performed, as proposed by Chang and Delleur [39, 40]. The well-known dataset Iris [41] in machine learning was used for this purpose. The ranges of the input parameter values were first defined during the sensitivity analysis. The size of the population was from the range [10, 200], while the coefficients' change range was on the interval [-1, 1]. The probability of mutation and of crossover were from the range [0.1, 1], and, finally, the number of individual evaluations from the interval [100, 10,000]. Taking these restrictions into account, 3,000 sets of parameter values were generated randomly, and the proposed genetic algorithm was evaluated accordingly. The obtained results were classified as acceptable if the run finished with a score of correctly predicted samples of more than 95%; otherwise the results were regarded as unacceptable. The cumulative frequencies were plotted of acceptable and unacceptable results. Insensitive parameters are characterized by similar cumulative frequencies of acceptable and unacceptable results throughout the whole range of parameter values. The following parameters were classified as insensitive: The probability of crossover, the probability of mutation, the coefficients' change range and the number of individual evaluations. On the other hand, the size of population was recognized as sensitive. In that case, a significantly larger number (approximately 30.2%) of acceptable results was achieved when its value was equal to 40 than in any other case. While influences of the sensitive parameters on the method's performance could be recognized straightforwardly, the optimal values of the insensitive parameters have to be tuned accordingly. In our case, a model-based approach with the linear regression was applied, as proposed in [42]. The selected optimal values for the genetic algorithm's parameters can be seen in Table 1.

Table 1. Parameters and their optimal values.

Parameter	Value
Probability of crossover	70 %
Probability of mutation	40 %
Size of the population	40
Number of individual evaluations	4,000
Coefficients' change range	[-0,2. 0.2]

3.2. Data Processing

Sentinel-2 data processing is a demanding and computer intensive process. An AMD Ryzen 5 4500U with 32 GB of main memory on Windows 10 was used for these reasons. In Fig. 3 we can see the exact location of Lake Cerknica in Slovenia. Fig. 4 shows the whole area of Lake Cerknica after the calculated WIW index and applied extraction mask. The Sentinel-2 data used for the calculation of WIW presented in Fig. 4 were acquired on 24 February, 2021. At that time, most of the lake was flooded with water (the blue pixels in Fig. 4), and only the east part and a small portion of the centre of the lake were dry.

Fig. 3. Location of Lake Cerknica in Slovenia.

Fig. 4. Area of Lake Cerknica, where blue pixels represent the flooded area of the lake.

Fig. 5 represents only the flooded parts of the lake. Recently, the flooded parts were converted from 2D to 3D, and, in that way, prepared for the calculation of the symmetry measure, which was calculated finally. The black line in Fig. 5 represents the plane of the 3D object of the flooded Lake Cerknica where the largest symmetry measure value was achieved. The calculated symmetry measure for the flooded parts in Fig. 5 was 1016.89. Then, the several different flooded areas of the lake were tested (see Fig. 6).

When the whole area of Lake Cerknica was flooded, the symmetry measure equaled 1,588.41, but, at the same time, when the lake was flooded less than presented in Fig. 5, the symmetry measures were also lower than in Fig. 5. An example of this can be seen in Fig. 6, where the symmetry measure was 983.77. This indicates that the lower the symmetry value is, the lower is the water level in Lake Cerknica. For the completely dry lake we assumed that the symmetry measure was equal to 0 and the surface elevation (above the sea level) was 541 m, while, at the surface level of 551 m, the symmetry measure was 1,588.41 (the whole lake was flooded). All the other calculated symmetry measures were in the mentioned range (from 0 to 1,588.41).

3.3. Interpretation of Prediction Model

The obtained prediction functions using the genetic algorithm presented in subsection 2.2 can be seen in Table 2.

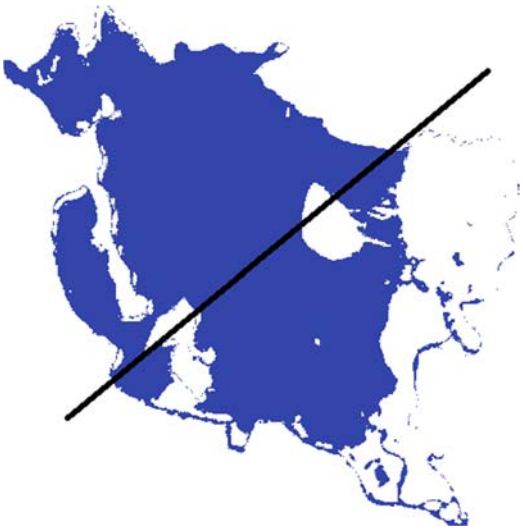

Fig. 5. Only the flooded area of Lake Cerknica, where the black line represents the largest symmetry value.

Fig. 6. Only a small part of the flooded area of Lake Cerknica, where the symmetry measure was 983.77.

Table 2. Prediction functions and their achieved RMSE.

ID	Prediction function	RMSE
1	$SE = -0.0042\ SM^3 + 4.1911\ SM^2 + 0.7824\ SM + 0.6433\ \sqrt{SM} + 0.2341$	0.9824
2	$SE = -0.0011\ SM^3 + 1.1708\ SM^2 - 4.6062\ SM - 4.5357\ \sqrt{SM} + 0.1523$	0.9963
3	$SE = -0.0012\ SM^3 + 1.1293\ SM^2 - 7.0471\ SM - 0.3752\ \sqrt{SM} + 0.2911$	1.0574
4	$SE = -0.0129\ SM^3 + 13.1534\ SM^2 - 1.4888\ SM + 0.4396\ \sqrt{SM} + 0.1472$	1.0641
5	$SE = -0.0028\ SM^3 + 2.9462\ SM^2 - 7.3371\ SM - 0.6071\ \sqrt{SM} + 0.0852$	1.0783
6	$SE = -0.0024\ SM^3 + 2.4943\ SM^2 + 9.0621\ SM + 3.2507\ \sqrt{SM} + 0.0513$	1.0969
7	$SE = -0.0018\ SM^3 + 1.8412\ SM^2 - 5.9313\ SM - 1.1612\ \sqrt{SM} + 0.0974$	1.1045
8	$SE = -0.0056\ SM^3 + 5.6911\ SM^2 - 5.9312\ SM - 1.1614\ \sqrt{SM} + 0.1692$	1.1103
9	$SE = -0.0034\ SM^3 + 3.4957\ SM^2 + 2.2993\ SM - 1.9101\ \sqrt{SM} + 0.1396$	1.1163
10	$SE = -0.0065\ SM^3 + 6.5582\ SM^2 - 4.7865\ SM - 2.4498\ \sqrt{SM} + 0.1623$	1.1201
11	$SE = -0.0043\ SM^3 + 4.8641\ SM^2 - 1.9744\ SM + 1.2902\ \sqrt{SM} + 0.4910$	1.1300
12	$SE = -0.0017\ SM^3 + 9.7071\ SM^2 + 2.3065\ SM - 0.0994\ \sqrt{SM} + 0.2901$	1.1309
13	$SE = -0.0052\ SM^3 + 3.8514\ SM^2 + 1.0087\ SM - 0.1851\ \sqrt{SM} + 0.1493$	1.1312
14	$SE = -0.0029\ SM^3 + 7.9763\ SM^2 - 2.6295\ SM + 0.9652\ \sqrt{SM} + 0.2475$	1.1331
15	$SE = -0.0038\ SM^3 + 1.5629\ SM^2 + 5.1702\ SM + 2.5801\ \sqrt{SM} + 0.6029$	1.1349

In all prediction functions SE represents the predicted Surface Elevation, and SM is the calculated Symmetry Measure. The performance of fitted functions was measured using RMSE. Using that type (predictive functions) of representation of a prediction model not only achieves very good results, but also allows us the interpretation of the learned functions. From the obtained functions it can be observed that all symmetry measures that were cubed (SM^3), have negative coefficients, which means that they have a negative influence on the final result. On the other hand, all squared (SM^2) symmetry measures have a positive influence due to their positive coefficients. In the case of symmetry measure (SM) and rooted symmetry measure ($\sqrt{SM}$) the influences are hard to explain, as some have negative, and some have positive coefficients. Finally, all the free coefficients have positive values and have positive influence on the final result. All the coefficients at SM^3 are very small and have small influence. There could be two main reasons: The first is that they do not have much influence, and the second, more likely, is due to the very large numbers that occur in the case of cubed values. Fifteen prediction functions with the highest achieved accuracies can be seen in Table 2. The smallest RMSE was equal to 0.9824, which means that the prediction error, on average, was less than one metre. As the difference between the lowest and highest surface elevations (above the sea level) is about 10 m, the achieved results show an error less than 10%, which is, if we take everything into account (Sentinel-2 resolution, shadows, clouds), a very good result.

4. Conclusion

The methodology for detection of water levels in the intermittent Lake Cerknica using a multispectral index acquired from Sentinel-2 and symmetry measure is presented in this paper. The results presented in the previous Section show that the symmetry measure of the 3D point cloud generated from the WIW index could be used for the prediction of water levels. The learned prediction functions achieved good results, and can be used for the prediction of surface levels. The use of ground truth data of the measured surface elevations of Lake Cerknica (e.g. sending experts to measure the exact elevation) and a bigger learning set (a combination of measured surface elevations and calculated symmetry measures), will be the main topic of the future work. The influence of other factors, such as shadows and clouds, on the quality of the WIW index will also be part of our future research work.

Acknowledgements

The authors acknowledge the financial support from the Slovenian Research Agency (Research Core Funding No. P2-0041 and Project No. N2-0181). This work was also supported by the Czech Science Foundation, Project 21-08009K Generalized Symmetries and Equivalences of Geometric Data.

References

[1]. Du Y., Zhang Y., Ling F., Wang Q., Li W., and Li X., Water bodies' mapping from Sentinel-2 imagery with modified normalized difference water index at 10-m spatial resolution produced by sharpening the SWIR band, *Remote Sensing*, Vol. 8, No. 4, 2016, p. 354.

[2]. Du N., Ottens H., and Sliuzas R., Spatial impact of urban expansion on surface water bodies: A case study of Wuhan, China, *Landscape and Urban Planning*, Vol. 94, No. 3, 2010, pp. 175-185.

[3]. Pekel J. F., Cottam A., Gorelick N., and Belward A. S., High-resolution mapping of global surface water and its long-term changes, *Nature*, Vol. 540, No. 7633, 2016, pp. 418-422.

[4]. Tulbure M. G. and Broich M., Spatiotemporal dynamic of surface water bodies using Landsat time-series data from 1999 to 2011, *ISPRS Journal of Photogrammetry and Remote Sensing*, Vol. 79, No. 1, 2013, pp. 44-52.

[5]. Singh K., Ghosh M., and Sharma S. R., WSB-DA: Water surface boundary detection algorithm using Landsat 8 OLI data, *IEEE Journal of Selected Topics in Applied Earth Observations and Remote Sensing,* Vol. 9, No. 1, 2015, pp. 363-368.

[6]. Acharya T. D., Lee D. H., Yang I. T., and Lee J. K., Identification of water bodies in a Landsat 8 OLI image using a J48 decision tree, *Sensors*, Vol. 16, No. 7, 2016, pp. 1075-1091.

[7]. Sivanpillai R. and Miller S. N., Improvements in mapping water bodies using ASTER data, *Ecological Informatics,* Vol. 5, No. 1, 2010, pp. 73-78.

[8]. Zhou Y., Luo J., Shen Z., Hu X., and Yang H., Multiscale water body extraction in urban environments from satellite images, *IEEE Journal of Selected Topics in Applied Earth Observations and Remote Sensing*, Vol. 7, No. 10, 2014, pp. 4301-4312.

[9]. Yang X., Zhao S., Qin X., Zhao N., and Liang L., Mapping of urban surface water bodies from Sentinel-2 MSI imagery at 10 m resolution via NDWI-based image sharpening, *Remote Sensing*, Vol. 9, No. 6, 2017, pp. 596-615.

[10]. Bhardwaj A., and Singh M. K., Joshi P. K., Singh S., Sam L., Gupta R. D., and Kumar R., A lake detection algorithm (LDA) using Landsat 8 data: A comparative approach in glacial environment, *International Journal of Applied Earth Observation and Geoinformation*, Vol. 28, No. 1, 2015, pp. 150-163.

[11]. Jiang H., Feng M., Zhu Y., Lu N., Huang J., and Xiao T., An automated method for extracting rivers and lakes from Landsat imagery, *Remote Sensing*, Vol. 6, No. 6, 2014, pp. 5067-5089.

[12]. Li W. and Gong P., Continuous monitoring of coastline dynamics in western Florida with a 30-year time series of Landsat imagery, *Remote Sensing of Environment*, Vol. 179, No. 1, 2016, pp. 196-209.

[13]. McFeeters S. K., The use of the normalized difference water index (NDWI) in the delineation of open water features, *International Journal of Remote Sensing*, Vol. 17, No. 7, 1996, pp. 1425-1432.

[14]. Ryu J.-H., Won J.-S., and Min K. D., Waterline extraction from Landsat TM data in a tidal flat: a case

study in Gomso Bay, Korea, *Remote Sensing of Environment*, Vol. 83, No. 3, 2002, pp. 442-456.
[15]. Yang X., Qin Q., Grussenmeyer P., and Koehl M., Urban surface water body detection with suppressed built-up noise based on water indices from Sentinel-2 MSI imagery, *Remote Sensing of Environment*, Vol. 219, No. 1, 2018, pp. 259-270.
[16]. Huang X., Xie C., Fang X., and Zhang L., Combining pixel-and object-based machine learning for identification of water-body types from urban high-resolution remote-sensing imagery, *IEEE Journal of Selected Topics in Applied Earth Observations and Remote Sensing*, Vol. 8, No. 5, 2015, pp. 2097-2110.
[17]. Xu H., Modification of normalised difference water index (NDWI) to enhance open water features in remotely sensed imagery, *International Journal of Remote Sensing,* Vol. 27, No. 14, 2006, pp. 3025-3033.
[18]. Feyisa G. L., Meilby H., Fensholt R., and Proud S. R., Automated water extraction index: a new technique for surface water mapping using Landsat imagery, *Remote Sensing of Environment*, Vol. 140, No. 1, 2014, pp. 23-35.
[19]. Lipman Y., Chen X., Daubechies I., and Funkhouser T., Symmetry factored embedding and distance, *ACM Transactions on Graphics*, 29, 4, 2010, p. 103.
[20]. Mitra N. J., Guibas L. J., and Pauly M., Partial and approximate symmetry detection for 3D geometry, *ACM Transactions on Graphics (TOG),* Vol. 25, No. 3, 2006, pp. 560-568.
[21]. Shi Z., Alliez P., Desbrun M. Bao H., and Huang J., Symmetry and orbit detection via lie-algebra voting, *Computer Graphics Forum*, Vol. 35, No. 5, 2016, pp. 217-227.
[22]. Sun C. and Sherrah J., 3D symmetry detection using the extended Gaussian image, *IEEE Transactions on Pattern Analysis and Machine Intelligence*, Vol. 19, No. 2, 1997, pp. 164-168.
[23]. Podolak J., Shilane P., Golovinskiy A., Rusinkiewicz S., and Funkhouser T., A planar-reflective symmetry transform for 3D shapes, *ACM SIGGRAPH 2006 Papers*, Vol. 1, No. 1, 2006, pp. 549-559.
[24]. Simari P., Kalogerakis E., and Singh K., Folding meshes: Hierarchical mesh segmentation based on planar symmetry, in *Proceedings of the Fourth Eurographics Symposium on Geometry Processing,* Cagliari, Sardinia, Italy, June 26-28, 2006, pp. 111-119.
[25]. Combes B., Hennessy R., Waddington J., Roberts N., and Prima S., Automatic symmetry plane estimation of bilateral objects in point clouds, in *Proceedings of the IEEE Conference on Computer Vision and Pattern Recognition*, 2008, pp. 1-8.
[26]. Sipiran I., Gregor R., and Schreck T., Approximate symmetry detection in partial 3D meshes, *Computer Graphics Forum*, Vol. 33, No. 7, 2014, pp. 131-140.
[27]. Li B., Johan H., Ye Y., and Lu Y., Efficient 3D reflection symmetry detection: A view-based approach, *Graphical Models*, Vol. 83, No. 1, 2016, pp. 2-14.
[28]. Speciale P., Oswald M. R., Cohen A., and Pollefeys M., A symmetry prior for convex variational 3D reconstruction, in *Proceedings of the European Conference on Computer Vision*, 2016, pp. 313-328.
[29]. Ecins A., Fermuller C., and Aloimonos Y., Detecting reflectional symmetries in 3D data through symmetrical fitting, in *Proceedings of the IEEE International Conference on Computer Vision Workshops,* 2017, pp. 1779-1783.
[30]. Nagar R. and Raman S., 3dsymm: robust and accurate 3D reflection symmetry detection, *Pattern Recognition,* Vol. 107, No. 1, 2020, p. 107483.
[31]. Hruda L., Kolingerova I., and Vaša L., Robust, fast and flexible symmetry plane detection based on differentiable symmetry measure, *The Visual Computer*, 2021, pp. 1-17.
[32]. Šmid H., Golež G., Podjed D., Kladnik D., Erhartič B., Pavlin P., and Jerele I., Encyclopedia of Natural and Cultural Heritage in Slovenia, Ljubljana, 2012.
[33]. Jesenko D., Hruda L., Kolingerova I., Žalik B., and Podgorelec D., Detection of water levels in Lake Cerknica using Sentinel-2 data and symmetry, in *Proceedings of the 3rd International Conference on Advances in Signal Processing and Artificial Intelligence,* 2021, pp. 65-69.
[34]. Lefebvre G., Davranche A., Willm L., Campagna J., Redmond, L., Merle C., Guelmami A., and Poulin B., Introducing WIW for detecting the presence of water in wetlands with landsat and sentinel satellites, *Remote Sensing*, Vol. 11, No. 19, 2019, p. 2210.
[35]. Wendland H., Piecewise polynomial, positive definite and compactly supported radial functions of minimal degree, *Advances in Computational Mathematics*, Vol. 4, No. 1, 1995, pp. 389-396.
[36]. Liu D. C. and Nocedal J., On the limited memory BFGS method for large scale optimization, *Mathematical Programming*, Vol. 45, No. 1, 1989, pp. 503-528.
[37]. Lešnik U, Mongus D., and Jesenko D., Predictive analytics of PM10 concentration levels using detailed traffic data, Transportation research. Part D, *Transport and Environment,* Vol. 67, No. 1, 2019, pp. 131-141.
[38]. Mongus D., Vilhar U., Skudnik M., Žalik, B., and Jesenko D., Predictive analytics of tree growth based on complex networks of tree competition, *Forest Ecology and Management,* Vol. 425, No. 1, 2018, pp. 164-176.
[39]. Chang F. J. and Delleur J. W., Systematic parameter estimation of watershed acidification model, *Hydological Processes*, Vol. 6, No. 1, 1992, pp. 29-44.
[40]. Jesenko D., Mernik M., Žalik B., and Mongus D., Two-level evolutionary algorithm for discovering relations between nodes' features in a complex network, *Applied Soft Computing*, Vol. 56, No. 1, 2017, pp. 82-93.
[41]. Blake C. L. and Merz C. J., UCI repository of machine learning databases, *University of California*, 1998, pp. 1-2.
[42]. Czarn A., MacNish C., Vijayan K., Turlach B., and Gupta R., Statistical exploratoryanalysis of genetic algorithms, *IEEE Transactions on Evolutionary Computation,* Vol. 8, No. 4, 2004, pp. 405-421.